Fuel Processing Technology 245 (2023) 107725

Contents lists available at ScienceDirect

Fuel Processing Technology

journal homepage: www.elsevier.com/locate/fuproc

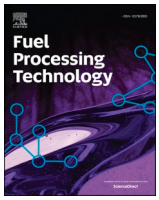

# Influence of feedstock variability on thermal decomposition of forest residue in a screw feeder for high temperature conversion

Nepu Saha [a], Jordan Klinger [a,*], Steven M. Rowland [b], Tim Dunning [b], Daniel Carpenter [b], Zach Mills [c], James Parks [c]

[a] Idaho National Laboratory, 1955 N. Fremont Avenue, Idaho Falls, ID 83415, USA
[b] National Renewable Energy Laboratory, 15013 Denver West Parkway, Golden, CO 80401, USA
[c] Oak Ridge National Laboratory, 1 Bethel Valley Rd, Oak Ridge, TN 37830, USA

ARTICLE INFO

*Keywords:*
High temperature conversion
Screw feeder
Feedstock compositional variability
Material deposition
Computational simulation

ABSTRACT

Thermochemical conversion of biomass uses high temperatures to break down the feedstock into products. Feeding the reactor, however, can be a challenge that impedes smooth operation of the thermochemical process. The aim of this study was to investigate the effect of feedstock compositional variability on the material deposition on the screw feeder during pyrolysis reactor feeding. Four different sample sets derived from pine (*Pinus Taeda*), 1st (rich in stem wood), 2nd (rich in bark and needles), 3rd (rich in stem wood), and 4th (whole residues), were used in this study while the reactor was operated at 500 °C. Results showed that the sample set consisted with cleaner feedstock experienced relatively less solid material and tar deposition on the screw feeder. For example, the lowest pseudo accumulation rate was 0.5 pitch/kg-feed for the 3rd set while the highest was 6.7 pitch/kg-feed for the 2nd set showing strong material dependance. Simulations on the temperature prediction inside the auger explored the surface of the auger exposed inside the reactor ($\Delta T_{avg}$ = 93 °C) and outlet of the purge gas region ($\Delta T_{avg}$ = 126 °C). This temperature drop would likely reduce the formation of deposits on the auger allowing the system for longer periods of continuous operation.

## 1. Introduction

Biomass is growing a huge interest to produce bioenergy, such as solid and liquid fuel, hydrogen energy, etc. Using biofuels (produced from energy crops) could significantly reduce greenhouse gas emission. An energy crop can have negative greenhouse gas emissions, meaning that carbon sequestration offsets emissions over the crop's life cycle [1,2]. For instance, corn stover can reduce emission by 90–103% [3]. However, due to the unfavorable physiochemical properties of biomasses, they need to undergo one or more treatments (e.g., chemical, thermochemical, biological, etc.) prior to use. Among all the treatments, thermochemical treatment (e.g., hydrothermal carbonization, torrefaction, pyrolysis, gasification, etc.) receives the most attention in the fuel production industries [4–9]. Feeding the reactor is one of the critical problems in all thermochemical treatments which impede smooth operation [10–12]. In general, the particle size and/or distribution relative to the equipment, the particle shape (which is responsible for particle-particle friction and interlocking, particle-wall friction), chemical composition, and moisture content are highly contributing to cohesive flow behaviors [13–18]. Due to having all these variabilities in the biomass feedstock, it become a huge challenge to feed at a constant rate. Various kinds of feeders, such as hopper systems, screw feeders, rotary valve feeders, piston feeders, belt feeders, vibratory feeders, rotary table feeders, etc. have been reported in the literature as feeding equipment in the thermochemical processes [10,19–22]. Among them screw (auger) feeder is one of the popular types because it can deliver bulk solids over a wide range of feedstocks and flowrates [10,21]. Dai et al. [21] tested a range of biomass materials and plastics in a screw feeder with crumbled pellets (rod, conical, and discal in shape) and some polyethylene particles (rounded) had similar particle size ranges. They found that the more irregular shapes led to a higher measured conveyance torque, but the results were nearly independent of conveyance speed. This suggests the flow behavior with respect to the power consumption may be well-correlated with dynamic flow friction. Dai and Grace [10] studied the effect of moisture content, particle size, and shape on the screw feeding where they found that large particles, wide

* Corresponding author.
*E-mail address:* jordan.klinger@inl.gov (J. Klinger).

https://doi.org/10.1016/j.fuproc.2023.107725
Received 30 September 2022; Received in revised form 14 February 2023; Accepted 28 February 2023
Available online 11 March 2023

size distributions, and high moisture contents generally led to blockage inside the screw resulting in an interruption of continuous flow. Miao et al. [22] noted that samples with a higher angle of repose (essentially the contact angle that a pile of the material makes with a surface when dispensed in a slow, low-stress quasi-static way) led to a higher volumetric efficiency, likely due to particle interlocking and high frictional effects. These impacts are intuitive for materials with high friction, but also likely lead to higher occurrences of feedstock plugging and jamming in feeders [23–26].

Most thermochemical conversion reactors are operated at high temperature where feedstock could experience elevated temperature even while they are in the feeder. During high temperature feeding, some of the physical (i.e., moisture content, particle size, and shape) and chemical (i.e., fiber composition) properties may change and result in potential for adhesion, cohesion, and carbon buildup. Variations in the molecular composition and porous microstructure of biopolymers directly impact the thermal properties that dictate optimal residence times [27,28]. As a result, thermally driven depolymerization (deposition of material) events occur at much shorter timescales than heat and mass transfer throughout biomass particles within the reactor. Thus, clogging to the feeder (interruption of continuous feed to the reactor) could be an unavoidable scenario. It is important to understand the changes in feedstock during the feeding operation in order to have the correct material attributes of the feedstock entering the conversion reactor unit to understand the potential clogging and other problems during this operation.

The aim of the study was to investigate how the feedstock compositional variability effects the material deposition on the screw feeder during feeding to a high temperature reactor unit. In addition, computational modeling was used to predict temperatures inside the feeder in the presence of different cooling systems. In this regard, the different fractions of pine (residues, stem wood, bark, and needles) were tested in a screw feeder while the pyrolysis reactor operated at 500 °C. Images were taken after the operation (before the next run) of the feeder and analyzed with ImageJ software to determine the material deposition during the operation. Computational modeling of the temperature profile of screw auger under different coolants (e.g., air, water) was conducted to optimize the pyrolysis reactor system.

## 2. Materials and methods

### 2.1. Materials

The feedstocks used in this study were commercially sourced from loblolly pine (*Pinus Taeda*) trees and were pre-processed at Idaho National Laboratory (INL) premises. Harvesting condition was “dry” with less than ½ inch of rainfall received within 10 days prior to harvest. Trees were prepared by the following: primary size reduction by chipping (Vermeer HG200), followed by subsequent size reduction stages in a high throughput hammer mill (Schutte Buffalo) with material retention sieves of decreasing size (6 mm followed by 2 mm), before the final size reduction and finishing in a knife mill (Thomas Wiley Model 4) with a 0.5 mm material retention sieve. The bulk materials (size reduced) were split with a series of riffle and rotary devices to provide similar materials to the National Renewable Energy Laboratory (NREL) for bio-oils production by using a 2″ fluidized bed reactor system (2FBR).

Physiochemical properties including the compositional analysis of the feedstocks are shown in Table 1, in addition to samples sets representing mass-averaged feedstock blends used in this study (further described in Section 2.2.1). Although the initial moisture content of the feedstocks was about 30 wt%, the samples were dried at 60 °C, which reduced the moisture content to 3–6% before thermal treatment. The ash content for the samples ranged from 0.29% (stem wood) to 3.91% (needles). Air classification of the residues resulted in a significant removal of ash, from a starting value of 1.52% to 0.95%. Air classification is a technique that uses an air stream to separate a material

**Table 1**
Feedstock characterizations in terms of moisture content, ultimate and proximate analysis, and compositional analysis.

| Feedstock | Moisture (wt%) | Volatiles (wt%) | Ash (wt %) | Fixed Carbon (wt%) | Hydrogen (wt%) | Carbon (wt%) | Nitrogen (wt%) | Oxygen (wt%) | Sulfur (wt%) | Water Extractable (wt%) | Ethanol Extractives (wt%) | Acetone Extractives (wt%) | Lignin (wt%) | Glucan (wt%) | Xylan (wt%) | Galactan (wt%) | Arabinan (wt%) | Mannan (wt%) | Acetyl (wt%) |
|---|---|---|---|---|---|---|---|---|---|---|---|---|---|---|---|---|---|---|---|
| Whole tree | 3.71 | 82.05 | 0.46 | 17.49 | 6.26 | 51.22 | 0.31 | 41.74 | 0.02 | 2.90 | 0.46 | 3.33 | 33.34 | 33.83 | 7.74 | 3.68 | 3.50 | 9.15 | 1.21 |
| Residues | 4.92 | 78.98 | 1.52 | 19.50 | 6.28 | 52.19 | 0.52 | 39.44 | 0.04 | 6.18 | 0.68 | 7.88 | 35.22 | 26.48 | 6.52 | 3.44 | 2.84 | 6.33 | 0.94 |
| Stem wood | 3.55 | 84.79 | 0.29 | 14.93 | 6.36 | 50.68 | 0.19 | 42.48 | 0.01 | 2.76 | 0.31 | 2.57 | 30.70 | 39.84 | 6.30 | 2.59 | 0.00 | 14.94 | 1.35 |
| Bark | 5.86 | 72.50 | 0.74 | 26.77 | 5.82 | 55.06 | 0.36 | 37.99 | 0.03 | 4.64 | 0.96 | 6.36 | 50.21 | 20.77 | 4.03 | 2.99 | 1.82 | 5.67 | 0.62 |
| Needles | 3.42 | 74.14 | 3.91 | 21.95 | 6.04 | 52.00 | 0.95 | 37.00 | 0.09 | 5.95 | 1.35 | 7.35 | 41.03 | 22.33 | 4.12 | 2.57 | 1.52 | 7.44 | 0.98 |
| Air classified residues* | 3.57 | 80.74 | 0.95 | 18.31 | 6.29 | 52.01 | 0.38 | 40.33 | 0.03 | 3.26 | 0.44 | 4.02 | 35.11 | 31.99 | 7.63 | 3.63 | 1.34 | 10.02 | 1.18 |
| 1st Sample Set | 3.55 | 83.98 | 0.42 | 15.61 | 6.35 | 50.95 | 0.23 | 42.05 | 0.01 | 2.86 | 0.34 | 2.86 | 31.58 | 38.27 | 6.57 | 2.80 | 0.27 | 13.96 | 1.32 |
| 2nd Sample Set | 4.49 | 77.20 | 1.62 | 21.18 | 6.12 | 52.55 | 0.53 | 39.14 | 0.04 | 4.96 | 0.84 | 6.28 | 39.43 | 26.10 | 5.72 | 3.20 | 2.48 | 7.14 | 0.94 |
| 3rd Sample Set | 3.64 | 83.19 | 0.39 | 16.42 | 6.30 | 51.00 | 0.26 | 42.05 | 0.02 | 2.84 | 0.40 | 3.01 | 32.24 | 36.33 | 7.14 | 3.23 | 2.04 | 11.46 | 1.27 |
| 4th Sample Set | 4.92 | 78.98 | 1.52 | 19.5 | 6.28 | 52.19 | 0.52 | 39.44 | 0.04 | 6.18 | 0.68 | 7.88 | 35.22 | 26.48 | 6.52 | 3.44 | 2.84 | 6.33 | 0.94 |

* Air classification was conducted for residues using a fan speed of 2.25 m/s.

stream according to their aerodynamic/drag properties, coupled with the size and density. This separation technique mainly leads to two fractions, such as heavies (considered as product) and lights (considered as reject) [4,29]. The light fraction mostly consists of lighter tissues, such as needles and bark, while the heavy fraction mostly consists of heavier tissues, such as stem wood. As the stem wood has relatively lower ash compared to needles and bark, the lower ash content in the air classified sample was expected. Similar to the ash, other chemical properties, such as volatiles, fixed carbon, elemental carbon and oxygen, extractives, lignin, glucan, and mannan contents were also varied between different samples. Interestingly, air classification of the residues resulted in a reduction of extractives and arabinan, and an apparent enrichment in cellulose (glucan) and mannan, likely due to loss of bark in the process.

## 2.2. Methods

### 2.2.1. Operation of 2FBR and material deposition on the auger

The studied materials were fed into a 2FBR using an auger feeder (see Supplementary Information Fig. S1). A detailed discussion of a similar reactor system has been presented in a previous study [30,31]. Briefly, the sample was fed by an auger feeder at a rate of 150–300 g/h into the fluidized bed, with a pyrolysis temperature of 500 °C. The temperature of the bed was maintained by fluidizing silica sand with 14 L/min nitrogen. Prior to analysis of the auger condition (in terms of material deposition), a 1.25–3.05 kg sample ran through the auger. A similar experiment was conducted through an auger with four different sample sets shown in Table 2. A picture was taken prior to cleaning the auger for the next run, and the material deposition on the auger was analyzed by using ImageJ software. In ImageJ, the auger flight was assumed to be a 2-dimensional projection. From the 2-dimensional projection, change in projected flight cross-sectional area with axial position and feedstock was measured. The data were corrected for non-ideal focal lengths based on tracking known auger geometries.

Table 2:Sample sets along with the feedstock, corresponding mass flowrate, and operation time.

| Sample set | Feedstock | Mass flowrate (g/h) | Operation time (h) |
|---|---|---|---|
| 1st Set | i. stem wood | 300 | 5.50 |
| | ii. air classified residues | 150 | 2.50 |
| 2nd Set | i. residues | 150 | 2.50 |
| | ii. whole tree | 150 | 2.50 |
| | iii. blend of bark and needles | 150 | 2.50 |
| | iv. 1:2:2 blend of residues with bark and needles | 150 | 2.50 |
| 3rd Set | i. stem wood | 300 | 4.20 |
| | ii. whole tree | 420 | 4.25 |
| 4th Set | i. residues | 300 | 4.17 |

The sample sets were selected and staged based on a larger matrix of materials to investigate feedstock variability, while minimizing the required amount of continuous pilot plant operation campaigns. This involved materials sets focused around loblolly pine, including, the main bole of the trees (stem wood), the residues left after lumber/pulpwood harvesting (residues), separated anatomical fractions from the residues (bark and needles) with higher inorganic species and extractives, as well as various blending combinations of these samples for additional compositional variance. For example, the 1:2:2 blend of the residues with additional bark and needles was intended to be indicative of a sample shipment to a biorefinery with excessive amount of these tissues (or some prolonged processing time with mixed composition). In a similar manner, the feedstock classes were grouped (sample sets) to have the highest impact with the fewest number of continuous pilot operation experiments. For example, the 1st sample set was clustered to see the impact of low inorganics and extractives, while the second and third sample sets were clustered to investigate the both a more mineral laden (2nd sample set) and less mineral laden (3rd sample set) samples compared to the as-harvested residues (4th), while having intermediate points of extractives contents, and overall having higher values of both inorganics and extractives than the relatively clean samples (1st sample set). Table 1 above shows the mass-averaged composition for each of the sample sets. The operating time was controlled to be >1 h to obtain a resolved mass balance, while some runs were maintained at longer times. The reactor feeder operated on a volumetric basis, and the resulting flow rate was an average phenomenological rate by weighing the initial/final feedstock (not a study parameter). These operating details are included for completeness, although the focus of this study normalizes the findings to the operating time/mass fed to compare average operational results.

### 2.2.2. Analysis of volatile compounds

To study the evolution of volatile compounds within the feed screws, the samples described in Table 1 were heated at temperatures of 200, 300, 400, and 500 °C in a quartz flow through reactor. The reactor was actively purged with a stream of helium, and the evolved gas was analyzed by molecular beam mass spectrometry (MBMS). A detailed description of the pyrolysis MBMS setup has be previously described [32].

### 2.2.3. Mechanical properties

The pine residues were thermally treated at 200 and 275 °C under inter environment to mimic the transformations of the biomass experiences during pyrolysis. Cyclic oedometer tests were performed to compare the relative compressibility and density evolution of the raw and thermally treated forest residues. These tests characterize the axial stress-strain relationships of materials during a cyclic compression and were adapted from ASTM E873–82 which was developed for particulate biomass. Material was added to the compression cell (114 mm) as loose as possible until the fill level height was approximately 66% of the cell's diameter. Cell agitation was minimized prior to loading in the load frame equipped with a 5 kN load cell (5982 Dual Column Floor Frame, Instron, Norwood, MA). The initial density was measured using an average bulk height at four separate locations, and the density evolution and axial strain was tracked using the displacement from the load frame which was maintained at a constant 5 mm/min. The applied axial stress was varied at 1, 2.5, 5.0, 7.5, and 10 kPa. The instantaneous elastic response of the bulk material was extracted as the bulk material began to relax after reaching the target stress and the piston retracted. The bulk modulus was then translated to the Young's Modulus with Poisson's ratio [33].

The material's internal friction and cohesion were measured using a ring shear tester (RST-01, Dietmar Schulze Schüttgutmesstechnik, Wolfenbüttel, Germany). Following ASTM D6773–08 the sample was loaded in a size M shear cell which is annular in cross-section with an inner diameter of 10 cm and outer diameter of 20 cm. The yield loci were constructed from a series of shear tests performed at pre-shear normal consolidation stresses of 1, 5, and 10 kPa. As the cell rotates slowly (0.02 rad/min), the quasistatic torque exerted on a veined, stationary lid is measured and converted to an average shear stress assuming uniform shear plane beneath the lid veins. These qualitative properties that indicate flow performance were measured to compare the impact of varying granular flow properties with potential competing flow impediments from reaction chemistry and liquid deposition, etc. [34].

### 2.2.4. Prediction of temperature profile inside the auger: A computer simulation

Computational simulations were performed using the conjugate heat transfer and fluid flow modules in COMSOL to understand the temperature profile along with the auger during the operation. The conjugate heat transfer module iteratively solves the energy equation in each

region of the domain (e.g., purge gas, coolant, auger, etc. regions) while utilizing temperature and heat flux information from contacting regions as boundary conditions. The inlet was approximated using a 2-dimensional axisymmetric domain, which significantly reduced computation time. In order to model the non-axisymmetric auger, using an axisymmetric domain, the density of the auger material was modified to ensure the total mass of the cylindrical shape matched that of the actual auger's helical shape. The region between the outer pipe and the reactor wall was treated as a solid with material properties approximating an air/sand/tar mixture. To avoid the need to model both the biomass and the purge gas between the auger and inner pipe, a single fluid, with properties approximating the mixture were used. Thermal boundary conditions used in the simulation are provided in Fig. 1. The temperature and heat transfer coefficient used along the exterior of the endcap and the auger tip were calculated based on the reactor operating conditions. A volumetric flowrate of 1.4 standard liter per minute (SLPM) used for the purge gas/biomass mixture. For simulations, using air as the cooling fluid (currently been used in the 2FBR biomass inlet), a pressure drop of 50 psi across the channel was used, and the k-epsilon model was used to model turbulence. For water, a velocity boundary condition of 0.5 m/s was used at the inlet, while the laminar flow did not require a turbulence model.

The biomass inlet used on the 2FBR, shown in Fig. 1, is constructed from three concentric pipes surrounding an auger. Biomass particles and purge gas are fed into the reactor between the auger and the inner pipe, while coolant flows between a channel formed by the three pipes and an endcap positioned at the end of the inner and outer pipes. The exterior of the endcap and about 6 mm of the auger are exposed inside the reactor. A heatshield is positioned between the inner and outer pipes within the coolant region to limit cooling of the endcap, which creates a region of static air between it and the outer pipe. Additionally, a gap exists between the reactor wall and the outer pipe, which is filled with an air/sand/tar mixture. Dimensions of these parts are provided in Table 3.

**Table 3**
Dimensions of biomass inlet. Note: N/A indicates the associated dimension is not applicable.

| Part | Inner radius (cm) | Outer radius (cm) | Length (cm) | Thickness (cm) |
|---|---|---|---|---|
| Outer pipe | 1.10 | 1.36 | 18.0 | N/A |
| Middle pipe | 0.87 | 1.00 | 15.8 | N/A |
| Inner pipe | 0.63 | 0.80 | 18.0 | N/A |
| Endcap | 0.63 | 1.36 | 0.25 | N/A |
| Auger | N/A | 0.48 | 18.6 | N/A |
| Heat shield | N/A | N/A | 1.90 | 0.17 |

## 3. Results and discussion

### 3.1. Effect of feedstock compositional variability on particle agglomeration

Fig. 2 shows photographs of the auger feeding the 2FBR reactor after several rounds of cleaning, focused on the flights near to the fluid bed contact zone (left edge of the photo). The top subplot (referred as 1st set of cleanouts) was taken after three days of testing with (1) stem wood, and (2) air classified, respectively. The feed rate for stem wood was 300 g/h and operated for 5.5 h. While the air classified sample fed for 2.5 h at a rate of 150 g/h. All these tests accumulated about 2.03 kg sample fed during this period. From the visual inspection, it can be seen that a significant accumulation of the feedstock and/or char on first ten flights of the auger following by minimal deposition. The second subplot from the top (referred as 2nd set of the cleanouts) was taken after four days of testing with (1) residues, (2) whole tree, (3) a blend of bark and needles, and (4) a 1:2:2 blend of residues with bark and needles, respectively. While these materials are distinctly different, these represent a collective of feedstocks with relatively higher ash and extractives content found in residues, bark, and needles. All four tests used a feed rate of 150 g/h and identical operating conditions and were run for 2.5 h totaling approximately 1.5 kg of sample fed in this cleanout cycle. It is clear from the visual inspection that, there was a significant deposit on approximately the first eight flights of the shaft which could be potential for clear process upsets through either plugging of the feeder and feeding agglomerated biomass aggregates to the fluid bed decreasing efficiency and potentially leading to bed instabilities. The third subplot from the top (referred as 3rd set of cleanouts) was taken after two days of testing with (1) stem wood, and (2) whole tree. These were fed at a comparatively faster rate of 300 and 420 g/h for 4.2 and 4.25 h respectively totaling approximately 3.05 kg of feedstock fed in this period. This was approximately a 40/60 split between a relatively clean feedstock (stem wood) and a residual feedstock. From visual inspection, there was relatively little accumulation of char on the auger shaft, with the deposit appearing with a less severely decomposed char. The bottom subplot (referred as 4th set of cleanouts) was taken out after two additional days of testing. Residues were fed in both days at rates of 300 g/h for 2.67 and 1.5 h respectively totaling 1.25 kg fed in this period. Interestingly the accumulation in this test appears close to the native color of the feedstock and suggests very little degradation- at least at the surface layer. Similar to the prior test, the deposit is observed in the first few pitches, but quickly decreases to a very thin layer.

In an attempt to understand the deposition/accumulation of material better, these images were digitally analyzed with ImageJ to measure the change in projected flight cross-sectional area with axial position and feedstock (see Supplementary Information Fig. S2). These areas of the 2-dimensional projections of the flights and material accumulation were exported for subsequent analysis. The results from these trials are shown in Fig. 3 and show a semi-quantitative evaluation of the accumulation over the test. The dashed lines in the plot represent a three-point moving average of the data points and smooth the trend with respect to the subjective evaluation of where each flight begins/ends in the

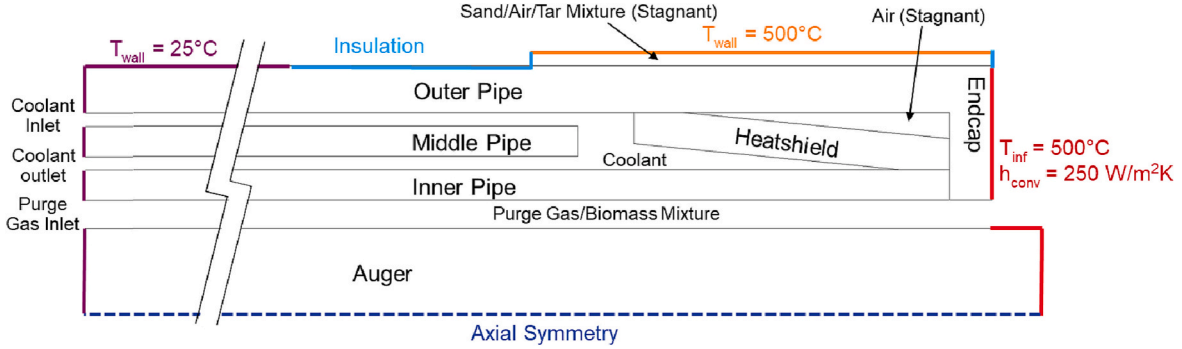


**Fig. 1.** 2-dimensional axisymmetric simulation domain used to model biomass inlet, with temperature boundary conditions applied.

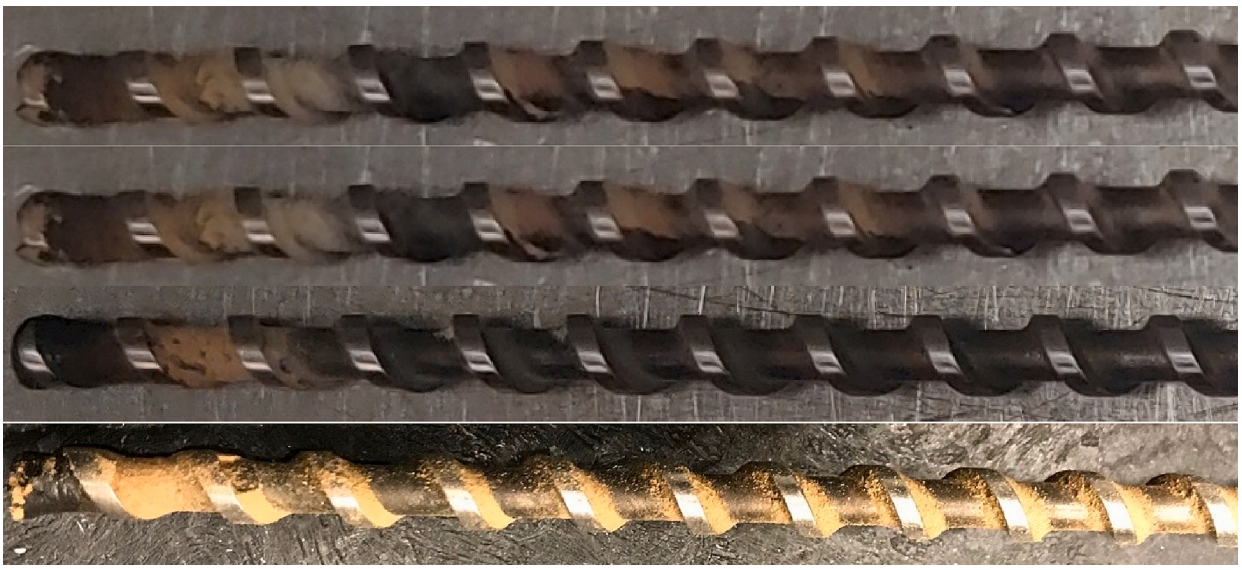

**Fig. 2.** Auger profiles from 1st set (TOP), 2nd set (2nd from the TOP), 3rd set (2nd from the BOT), and 4th set (BOT) cleanouts.

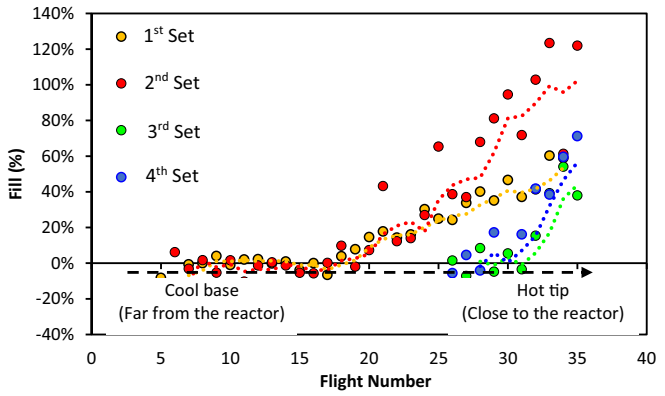


**Fig. 3.** Accumulation rate for three clean out during variability runs. The data points represent approximate fill percentage based on image analysis and the dashed lines show a 3-point moving average of the data to smooth measurement error between flight determinations.

photographs. As evident, the first cleanout showed about 60% of the filling near to the reactor. On the other hand, the cleanout of the second set was very nearly at a feeding upset event with the last few flights approximately 100% full. This accumulation persisted for approximately 10 flights down the axial length. Subsequently, the other two cleanouts showed very similar results with the maximum filling approaching 40–60% that decayed to a clean shaft after 3–5 flights.

Integrating these results for the length of the auger, the 1st cleanout had approximately 5.5 full pitch volumes deposited, while the 2nd 3rd, and 4th had 10.1, 1.5, and 2.3 pitch volumes of deposit respectively. This leads a pseudo accumulation rate of 2.7 pitch/kg, 6.7 pitch/kg, 0.5 pitch/kg, and 1.8 pitch/kg respectively for the cases in the particular feed system. Comparatively, for the four cases, the second test had the highest accumulation rate, used the slowest feed rate, and had feedstock potentially with the poorest quality attributes (high ash, high extractives). The second highest accumulation rate was observed for the first set where moderate feed rate of stem wood and air classified material was maintained. This feedstock has the highest hemicellulose along with the moderated extractives which could degrade or deformed near the reactor side of the auger (where the temperature is relatively high) and deposit on the flight. The lowest accumulation was observed in the third set cleanout that used a high proportion of stem wood for the tests as well as a higher feed rate. Previously Thanh et al. [35] reported that the condensable species from various pine anatomical fractions showed the potential for significant condensable, "sticky" tars, waxes, and terpenes that are hypothesized to contribute to these feeding failures. In particular, these were linked to the tissues present in high concentrations in the first studied case and support the hypothesis. Although 3rd set was conducted for relatively longer time at higher flowrate compared to 4th set, their deposition behaviors were similar. This could be due to the presence of a fairly significant amount of clean feedstock (about 40%) in 3rd set that makes smaller amount of sticky products resulting in relatively less material deposition on the flight. Typically, pine species contain organic acids that comprise a major portion of the resin [36,37], a sticky substance that is present in the outer cells which could be one potential contribution to adhesion in the screw feeder, even at relatively low temperatures.

### 3.2. Compressibility and shear properties of thermally modified material

To mimic the transformations of the biomass experiences after undergoing various thermal environments at 200 °C and 275 °C as it is conveyed to the 2FBR, these samples were tested for bulk properties. The elastic-strain behavior of the raw pine and the thermally treated pines shown in Fig. 4. Overall, the thermally treated bulk grains experience similar strain but are more easily consolidated. As the temperature environment was increased in severity, the measured bulk modulus decreased at the same stress conditions, indicating a significantly decreased elastic response of the material upon changing stress-state. This could be a result of partial particle fragmentation and altered surface friction and structure damage. Interestingly the strain-dependence of the modulus appears to approach that of the initially wet material, although here again the modulus values are significantly lower at similar loading conditions. This indicates that as the material is thermally treated, there is a tendency of the material to behave less elastically but have a similar overall modulus-strain relationship at high leading conditions. If there was to be accumulation of some plug formation that constricts the flow of pine granules, the thermally treated materials would tend to behave and consolidate/respond to compressive forces more similar to the way to wet (~30%) pine rather than the initial dry material.

The measured internal friction of the thermally treated samples was not significantly different from that of dry pine (41°) shown in Fig. 5. The cohesion was 1.2 kPa at 10 kPa pre-shear, dropping to 0.4 kPa at 5

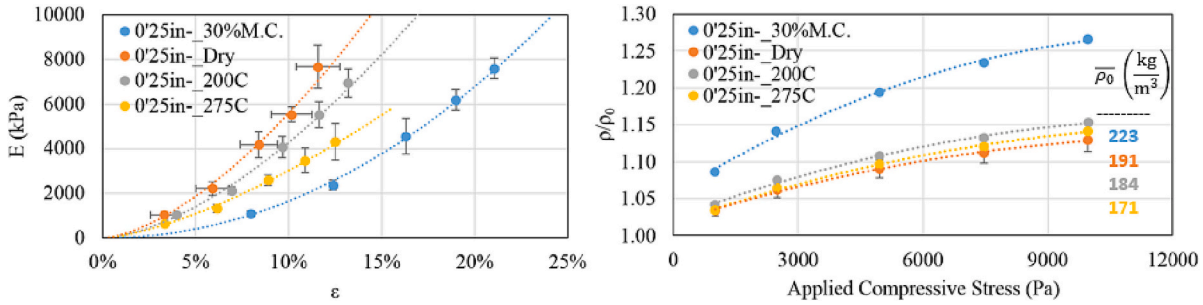


**Fig. 4.** Cyclic oedometer tests of the pine samples. Average elasticity modulus on the left while average relative density evolution on the right.

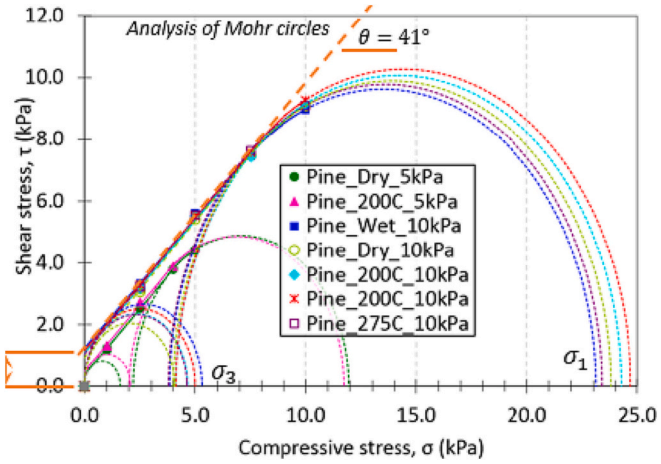


**Fig. 5.** Schulze Ring Shear testing and Mohr circle analysis of pine samples.

kPa pre-shear. Overall, Mohr-Coulomb yield envelops, and criterion are insufficient to describe differences in bulk failure observed from flow testing of the materials, and do not help illuminate the measured differences in the consolidation testing described above. This could suggest, again, that flowability issues with respect to the material being fed into the 2FBR are not necessarily a result of bulk flow phenomena, but rather an issue related to the inherent changes of material's compressible/elastic response as it partially decomposes. With a decreased elastic response and spring back, there may be a tendency to for granules to more easily accumulate and compress, forming plugs.

### 3.3. Evaluation of volatile components during feed screw operation

To understand the evolution of volatile components from the studied samples at temperatures that are relevant to feed screw operation, we studied the MBMS. Results showed that between 200 and 300 °C the evolution of diterpenoids (resin acids), that have previously been identified in loblolly pine extracts [38]. Since pine residue is comprised of many parts of the tree, it is difficult to discern if any one component is most responsible for feed screw plugging. As a result, volatiles analysis of anatomical fractions was conducted to understand the role of each component.

All spectra for the whole forest residue and the anatomical fractions were analyzed by multivariate curve resolution (MCR). MCR deconvolves unresolved spectral components to provide the spectra of the "pure" components. This analysis yielded three component spectra that corelate with the spectral differences observed as a function of temperature. Fig. 6 shows the components for the whole forest residue, with the component spectra on the left and the concentrations at the measured temperatures on the right. For the forest residue, component 1 is primarily observed at 200 and 300 °C and is comprised of light gasses, such as $CO_2$ and water vapor, as well as diterpenoids (resin acids). These

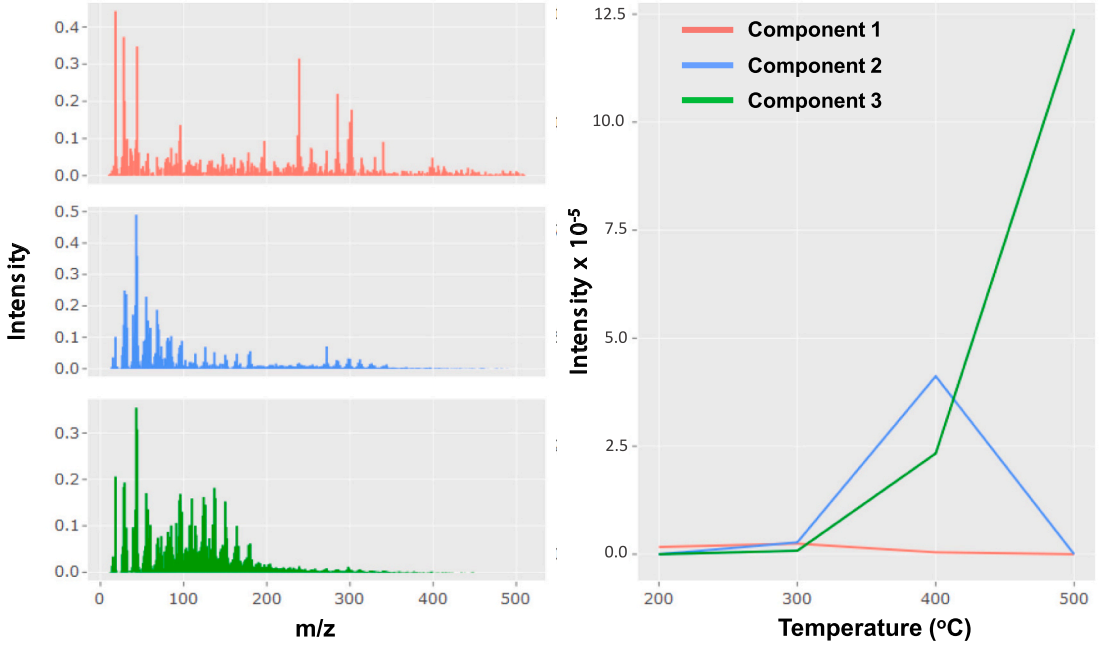


**Fig. 6.** Results from MCR analysis for whole forest residue. Three very distinct components were observed that correspond to the measured temperature regimes.

resin acids are known to be very sticky and viscous, and they can harden to rosin, which is commonly used to increase friction. We observe similar compositions from 200 to 300 °C in all the anatomical fractions. Component 2, which is primarily contributed to 400 °C treatment reveals high molecular weight compounds, albeit at different masses and intensity ratios compared to the 200–300 °C data, as well as lignin monomers, and cellulose breakdown products. Finally, component 3 resembles the spectra observed by pyrolysis at 500 °C. These results indicate both the presence of terpenoids at temperatures <300 °C and the onset of pyrolysis at temperatures of 400 °C or less. Both of these aspects are relevant to the production release of "sticky" chemicals that can lead to particle adhesion and cohesion.

Some differences in the early volatiles were observed between the anatomical fractions at 200 and 300 °C. Fig. 7 shows the mass spectra from thermal treatment at 200 °C. Most of the peaks shown have been linked to diterpenoids; however, the origin of spectral peaks observed at *m/z* values >302 are unknown. They are likely due to other compounds present in the pine resin. Further investigation is needed to understand the composition of these peaks.

### 3.4. Computational modeling to predict temperatures inside the biomass inlet

The auger feeding the biomass into 2FBR usually experiences stalling when the pyrolysis system operating continuously for multiple hours. This is due to high temperatures in the biomass inlet leading to the biomass particles pyrolyzing while still inside the auger. The pyrolysis of the particles leads to the formation of deposits along the biomass inlet and agglomeration of particles. This increases friction between the auger and the walls of the inlet, requiring more torque from the motor driving the auger. With sufficiently high friction, the motor is unable to produce enough torque and stalls. Once stalling occurs, the reactor must be shut down and the auger removed and cleaned. In order to limit the rate at which this occurs, computational modeling was used to predict temperatures inside the biomass inlet, and investigate methods for reducing these temperatures and, subsequently, the formation of deposits leading to motor stalling.

With air as the coolant, temperatures along the surface of the auger and at the outlet of the purge gas/biomass region reach as high as 379 °C and 491 °C, respectively, which can be seen in the top of Fig. 8. This is sufficiently high for pyrolysis to occur inside the inlet, leading to the formation of deposits which eventually cause motor stalling, exactly the same thing observed in Section 3.1. These high temperatures are due to the low density and heat capacity of air, which makes it not ideal for use as a coolant. Based on the poor performance of air, the effect of switching the coolant to water was investigated. The resulting temperature distributions in the biomass inlet with water as the coolant can be seen in the bottom of Fig. 8. Switching to water for the coolant showed significantly reduce the temperatures in both the surface of the auger exposed inside the reactor ($\Delta T_{avg} = 93$ °C, $\Delta T_{max} = 97$ °C) and outlet of the purge gas region ($\Delta T_{avg} = 126$ °C, $\Delta T_{max} = 103$ °C) of the inlet. This drop in temperature would likely reduce the rate at which deposits forms on the auger causing the motor to stall. A drawback of this increase in cooling provided by the water is the lower endcap temperature ($\Delta T_{avg} = 86$ °C, $\Delta T_{max} = 71$ °C), which would result in a cold region within the reactor. The average and maximum temperatures in the auger, endcap, and purge gas regions for both air and water coolants are provided in Table 4.

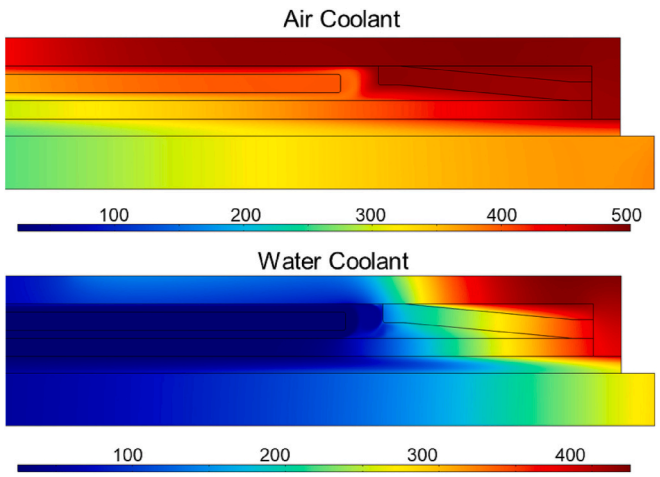


**Fig. 8.** Temperature distributions in biomass inlet with air (top) and water (bottom) as cooling fluid.

There are several reactor design criteria that could help prevent the occurrence of cold spots in the reactor. These include increasing the heat flux to the reactor through increased superficial velocity, increasing the thermal mass inside the bed by increasing the ratio of bed material to the biomass loading, or redesigning the coupling between the feeder and the reactor bed. The later suggestion, for example, could include using a variable pitch screw (longer pitch) nearer to the reactor bed where the biomass is effectively feed much faster in that zone. This would lessen the amount of thermal transfer between the screw/housing and the biomass feedstock. This would also relax the requirement of the close spatial coupling between the cooling jacket and the reactor body and thereby the occurrence of cold spots.

The effect of varying the coolant flowrate on the inlet temperatures was investigated while the water was utilized as the coolant as it showed improved cooling in the earlier discussion. Five simulations were

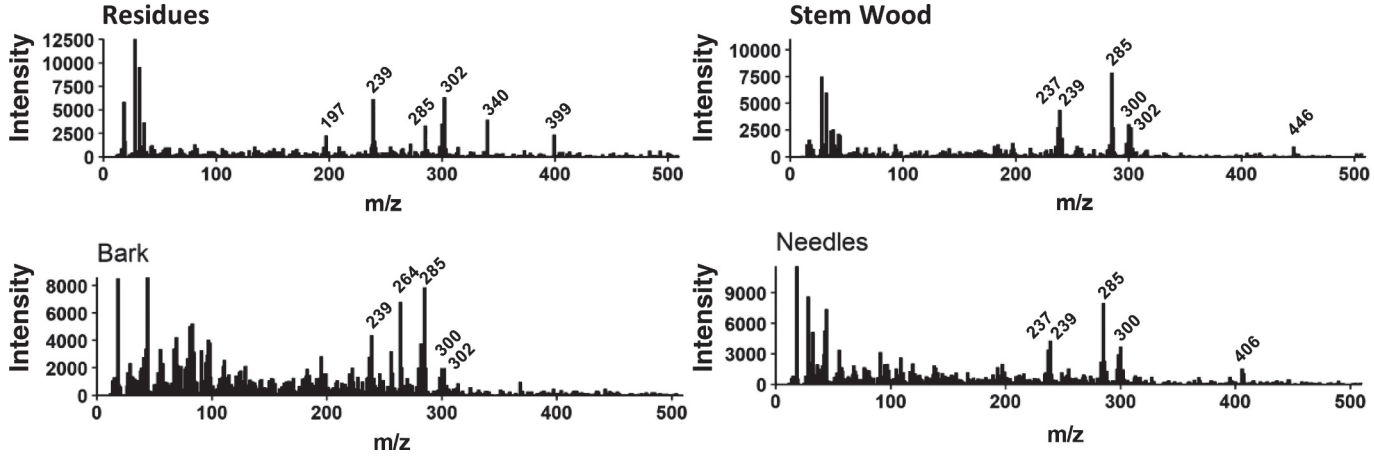


**Fig. 7.** Mass spectra from MBMS analysis at 200 °C. Values of m/z for the most abundant diterpenoid peaks, as well as high molecular weight unknowns, are shown.

**Table 4**
Average and maximum temperatures in auger, endcap, and purge gas regions of biomass inlet using air and water coolants. Note: Average and maximum temperatures are calculated at the outlet of the purge gas/biomass regions and the surfaces of the endcap and auger exposed inside the reactor.

| Fluid | $T_{auger}$ (°C) | | $T_{endcap}$ (°C) | | $T_{purge}$ (°C) | |
|---|---|---|---|---|---|---|
| | Average | Maximum | Average | Maximum | Average | Maximum |
| Air | 375 | 379 | 488 | 491 | 428 | 483 |
| Water | 282 | 282 | 402 | 420 | 302 | 380 |

performed with the average velocity varying from 0.5 to 1.5 m/s. The resulting temperature distributions throughout the domain as well as the average and maximum temperatures in the auger, purge gas and end cap regions are provided in Fig. 9 and Table 5, respectively. It can be seen from this data that increasing the flowrate of coolant produces only small decreases in the inlet temperatures. This is because at an average velocity of 0.5 m/s, the water has sufficient thermal capacity to reduce the temperatures of the surfaces it contacts while undergoing only a small increase in temperature. Therefore, at higher flowrates the additional thermal capacity of the coolant produces minimal additional cooling in the system.

While switching from air to water for the coolant produces significantly lower temperatures in both the auger and purge gas/biomass regions of the inlet, these regions still reach temperatures at which deposits from the biomass can form along the auger and produce agglomeration in the particles. These temperatures occur close to the inside of the reactor where the heatshield produces a region of nearly stagnant flow. With the coolant nearly stagnant in this region, this section of the inlet undergoes minimal convective cooling, allowing it to reach temperatures significantly higher than the coolant inlet temperature. Because of this, the effect of reducing the length of the heatshield was investigated to determine its effect on the temperature distribution. The resulting temperature distributions throughout the domain as well as the average and maximum temperatures in the auger, purge gas and end cap regions are provided in Fig. 10 and Table 6, respectively. It can be seen that as the length of the heatshield and subsequently the region of stagnant fluid decreases, the temperatures in the purge gas and auger near the inlet exit are reduced as well. By completely removing the heatshield, the average temperatures along the tip of the auger and the outlet of the purge gas are reduced by 28 °C and 168 °C, while the maximum temperatures were reduced by 28 °C and 151 °C, respectively. This comes at the cost of significantly lower average and maximum temperatures along the reactor side of the endcap which decreased by 273 °C and 256 °C, respectively. Because of this corresponding drop in endcap temperature, if the heatshield is redesigned to improve cooling of the purge gas and auger, its effect on the endcap temperature must be considered to ensure it does not negatively impact the reactor performance.

As shown in the previous section it is desirable to maintain biomass exposure temperature below 250–300 °C, thereby avoiding decomposition in the screw feeder leading char or tar accumulations. From Fig. 10, it is clear that the absent or very short heat shield length leads to the coldest endcap temperature although maintains the lowest screw temperature. Conversely, the longest heat shield results in the hottest endcap temperature (less chance to draw heat from the reactor) but also exposes the biomass in the feed screw to a warmer temperature gradient for a longer period as the heat conducts back up the length of the feed barrel. Additional design concepts to decouple the cooling jacket or more complex heat shield geometries could further improve the performance.

## 4. Conclusions

The early volatiles, corresponding predominately to diterpene resin acids, were observed at temperatures as low as 200 °C. Each anatomical fraction showed slightly different abundances for resin acid peaks, which may indicate different resin acid compositions; however, these compounds were observed in all anatomical fractions. It can be concluded that cleaner the feedstock, slower material deposition on the screw, resulting in a smooth flow. It is also suggestive from these tests

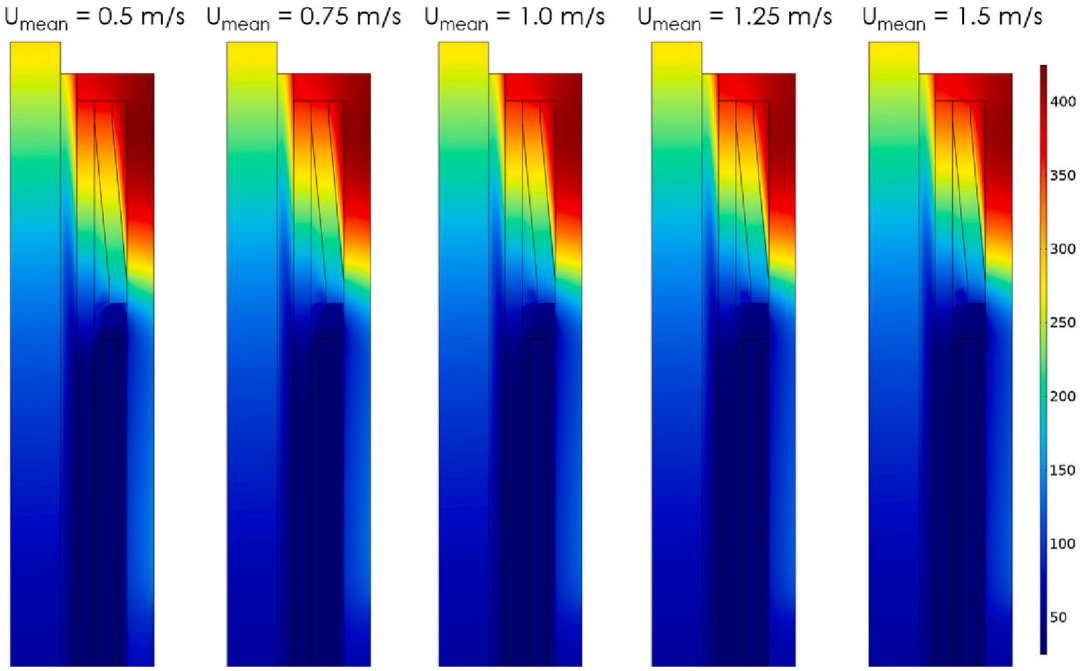


**Fig. 9.** Temperature distributions in biomass inlet with varying flowrates of water coolant.

**Table 5**
Average and maximum temperatures in auger, endcap, and purge regions of biomass inlet with varying flowrates of water coolant. Note: Average and maximum temperatures are calculated at the outlet of the purge gas/biomass regions and the surfaces of the endcap and auger exposed inside the reactor.

| $U_{mean}$ (m/s) | $T_{auger}$ (°C) | | $T_{endcap}$ (°C) | | $T_{purge}$ (°C) | |
|---|---|---|---|---|---|---|
| | Average | Maximum | Average | Maximum | Average | Maximum |
| 0.50 | 282 | 282 | 402 | 420 | 302 | 380 |
| 0.75 | 280 | 280 | 398 | 418 | 297 | 375 |
| 1.00 | 279 | 279 | 395 | 416 | 294 | 371 |
| 1.25 | 278 | 279 | 398 | 414 | 292 | 370 |
| 1.50 | 278 | 278 | 392 | 413 | 291 | 368 |

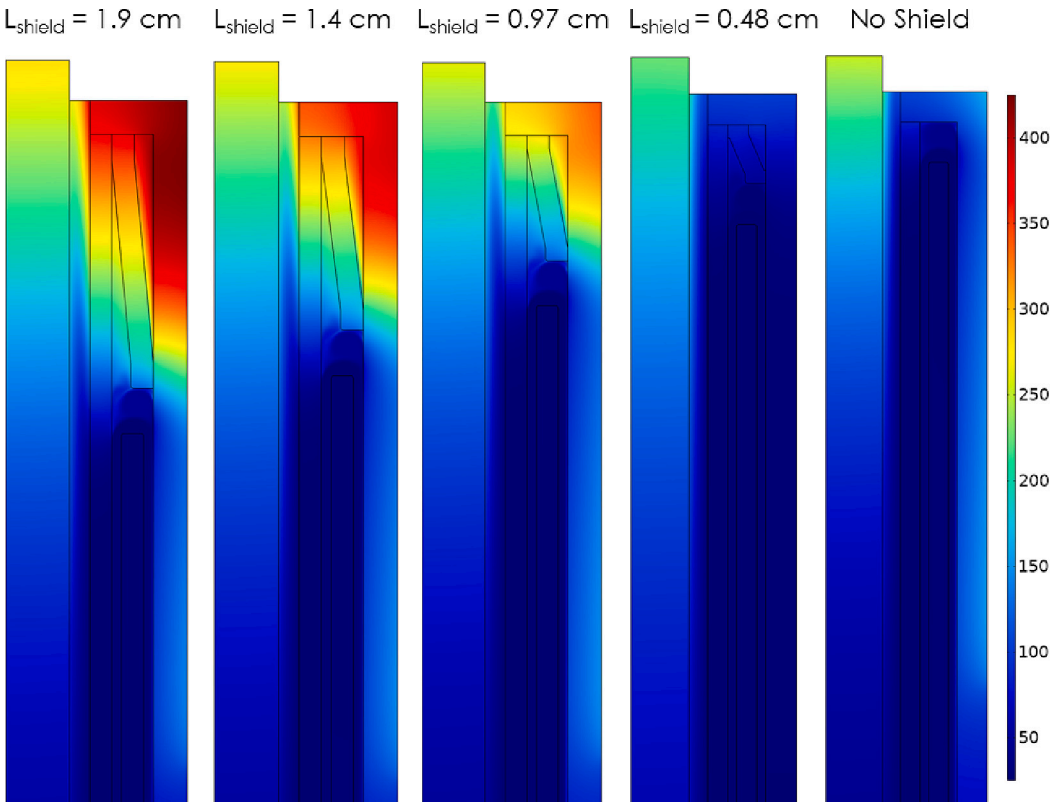


**Fig. 10.** Temperature distributions in biomass inlet with varying heatshield lengths (coolant fluid is water).

**Table 6**
Average and maximum temperatures in auger, endcap, and purge regions of biomass inlet with varying endcap heatshield length (coolant fluid is water). Note: Average and maximum temperatures are calculated at the outlet of the purge gas/biomass regions and the surfaces of the endcap and auger exposed inside the reactor.

| $L_{shield}$ (cm) | $T_{auger}$ (°C) | | $T_{endcap}$ (°C) | | $T_{purge}$ (°C) | |
|---|---|---|---|---|---|---|
| | Average | Maximum | Average | Maximum | Average | Maximum |
| 1.9 | 282 | 282 | 402 | 420 | 302 | 380 |
| 1.4 | 271 | 271 | 366 | 389 | 269 | 340 |
| 0.97 | 263 | 263 | 313 | 340 | 229 | 285 |
| 0.48 | 254 | 255 | 102 | 103 | 135 | 230 |
| No shield | 254 | 254 | 129 | 164 | 134 | 229 |

that the feed rate also plays a potential role in these phenomena. In general, there are inefficiencies in material transport in screw conveyors that led to poor conveyance with low filling. This can be the result of geometry clearance, or the slippage of particles past auger flights in the absence of a bulk mass to promote material transport.

Numerical simulations suggested that the purge gas and biomass mixture, as well as the auger conveying the biomass reach temperatures as high as 491 °C and 379 °C, respectively when air is used as the coolant. These temperatures are sufficiently high for the biomass to begin pyrolyzing inside inlet, leading to the formation of deposits, which eventually cause stalling in the auger motor. Switching the coolant from air to water could provide a temperature decrease of nearly 100 °C in the biomass as it traveled along the auger. The improved cooling of the inlet at the cost of lower endcap temperatures, the average of which decreases to around 400 °C. This lower temperature on the surface of the endcap exposed inside the reactor increases the likelihood of deposits forming on it. However, the reduction in biomass temperatures, and subsequently the formation of deposit on the auger, outweigh this potentially adverse effect. The influence of coolant flowrate and heatshield design showed that due to the significantly higher thermal capacity of the water

compared to the purge gas/biomass mixture, increasing its flowrate produced minimal additional cooling in the system. The length of the heatshield, however, has a large influence on temperatures in sections of the inlet positioned near the reactor.

Although these tests and simulations are not completely decoupled of feed rate and feedstock quality attributes, it presents significant differences between the trials and requires further study.

## CRediT authorship contribution statement

**Nepu Saha:** Data curation, Formal analysis, Methodology, Writing – original draft. **Jordan Klinger:** Conceptualization, Data curation, Formal analysis, Funding acquisition, Supervision, Writing – review & editing. **Steven M. Rowland:** Data curation, Formal analysis, Methodology, Writing – review & editing. **Tim Dunning:** Data curation, Methodology, Writing – review & editing. **Daniel Carpenter:** Data curation, Conceptualization, Funding acquisition, Supervision, Writing – review & editing. **Zach Mills:** Formal analysis, Methodology, Software, Writing – review & editing. **James Parks:** Conceptualization, Formal analysis, Funding acquisition, Supervision, Software, Writing – review & editing.

## Declaration of Competing Interest

The authors declare that they have no known competing financial interests or personal relationships that could have appeared to influence the work reported in this paper.

## Data availability

Data will be made available on request.

## Acknowledgment

The research is supported by the U.S. Department of Energy (DOE), Office of Energy Efficiency and Renewable Energy (EERE), Bioenergy Technologies Office (BETO), under DOE Idaho Operations Office with Contract No. DE-AC07-05ID14517.

## Appendix A. Supplementary data

Supplementary data to this article can be found online at https://doi.org/10.1016/j.fuproc.2023.107725.

## References

[1] C.R. Locker, S. Torkamani, I.J. Laurenzi, V.L. Jin, M.R. Schmer, D.L. Karlen, Field-to-farm gate greenhouse gas emissions from corn Stover production in the Midwestern U.S, J. Clean. Prod. 226 (2019) 1116–1127.
[2] J. McKechnie, M. Pourbafrani, B.A. Saville, H.L. MacLean, Exploring impacts of process technology development and regional factors on life cycle greenhouse gas emissions of corn Stover ethanol, Renew. Energy 76 (2015) 726–734.
[3] R. Chillrud, Biofuels versus Gasoline: The Emissions Gap is Widening, Environmental and Energy Study Institute, 2016.
[4] M.T. Islam, N. Saha, S. Hernandez, J. Klinger, M.T. Reza, Integration of air classification and hydrothermal carbonization to enhance energy recovery of corn stover, Energies 14 (2021) 1397.
[5] S. Szufa, Ł. Adrian, P. Piersa, Z. Romanowska-Duda, M. Grzesik, A. Cebula, S. Kowalczyk, Experimental studies on energy crops torrefaction process using batch reactor to estimate torrefaction temperature and residence time, in: Renewable Energy Sources: Engineering, Technology, Innovation, Springer, 2018, pp. 365–373.
[6] M.T. Domínguez, P. Madejón, E. Madejón, M.J. Diaz, Novel energy crops for Mediterranean contaminated lands: Valorization of *Dittrichia viscosa* and *Silybum marianum* biomass by pyrolysis, Chemosphere 186 (2017) 968–976.
[7] N. Saha, E. Fillerup, B. Thomas, C. Pilgrim, T. Causer, D. Herren, J. Klinger, Improving bamboo's fuel and storage properties with a net energy export through torrefaction paired with catalytic oxidation, Chem. Eng. J. 440 (2022), 135750.
[8] E. Hu, C. Dai, Y. Tian, Y. Yang, X. Yi, M. Li, S. Shao, Y. Zhao, Infrared heated pyrolysis of corn Stover: Determination of kinetic and thermodynamic parameters, J. Anal. Appl. Pyrolysis 158 (2021), 105273.
[9] A.E.M. Fodah, M.K. Ghosal, D. Behera, Quality assessment of bio-oil and biochar from microwave-assisted pyrolysis of corn Stover using different adsorbents, J. Energy Inst. 98 (2021) 63–76.
[10] J. Dai, J.R. Grace, Biomass granular screw feeding: an experimental investigation, Biomass Bioenergy 35 (2011) 942–955.
[11] G. Lian, W. Zhong, X. Liu, DEM study on the mixed feeding process of coal and cylindroid biomass particles in a screw feeder, Adv. Powder Technol. 32 (2021) 2543–2554.
[12] G. Wehner, A. Schikora, F. Ordon, T. Will, Priming negatively affects feeding behaviour and aphid biomass of *Rhopalosiphum padi* on barley, J. Pest. Sci. 94 (2021) 1237–1247.
[13] A.M.N. Faqih, A. Mehrotra, S.V. Hammond, F.J. Muzzio, Effect of moisture and magnesium stearate concentration on flow properties of cohesive granular materials, Int. J. Pharm. 336 (2007) 338–345.
[14] K. Siliveru, R.K. Ambrose, P.V. Vadlani, Significance of composition and particle size on the shear flow properties of wheat flour, J. Sci. Food Agric. 97 (2017) 2300–2306.
[15] H. Shi, R. Mohanty, S. Chakravarty, R. Cabiscol, M. Morgeneyer, H. Zetzener, J. Y. Ooi, A. Kwade, S. Luding, V. Magnanimo, Effect of particle size and cohesion on powder yielding and flow, KONA Powd. Part. J. (2018) 2018014.
[16] V. Vivacqua, A. López, R. Hammond, M. Ghadiri, DEM analysis of the effect of particle shape, cohesion and strain rate on powder rheometry, Powder Technol. 342 (2019) 653–663.
[17] J. Wang, H. Yu, P. Langston, F. Fraige, Particle shape effects in discrete element modelling of cohesive angular particles, Granul. Matter 13 (2011) 1–12.
[18] N. Saha, C. Goates, S. Hernandez, W. Jin, T. Westover, J. Klinger, Characterization of particle size and moisture content effects on mechanical and feeding behavior of milled corn (*Zea mays* L.) stover, Powder Technol. 405 (2022) 117535.
[19] A. Van der Drift, H. Boerrigter, B. Coda, M. Cieplik, K. Hemmes, Entrained flow gasification of biomass, in: Ash Behaviour, Feeding Issues, System Analyses, 2004.
[20] K.R. Cummer, R.C. Brown, Ancillary equipment for biomass gasification, Biomass Bioenergy 23 (2002) 113–128.
[21] J. Dai, H. Cui, J.R. Grace, Biomass feeding for thermochemical reactors, Prog. Energy Combust. Sci. 38 (2012) 716–736.
[22] Z. Miao, T.E. Grift, A.C. Hansen, K.C. Ting, Flow performance of ground biomass in a commercial auger, Powder Technol. 267 (2014) 354–361.
[23] Y. Lu, W. Jin, J. Klinger, S. Dai, Flow and arching of biomass particles in wedge-shaped hoppers, ACS Sustain. Chem. Eng. 9 (2021) 15303–15314.
[24] Z. Cheng, J.H. Leal, C.E. Hartford, J.W. Carson, B.S. Donohoe, D.A. Craig, Y. Xia, R. C. Daniel, O.O. Ajayi, T.A. Semelsberger, Flow behavior characterization of biomass Feedstocks, Powder Technol. 387 (2021) 156–180.
[25] D. Ilic, K. Williams, R. Farnish, E. Webb, G. Liu, On the challenges facing the handling of solid biomass feedstocks, Biofuels Bioprod. Biorefin. 12 (2018) 187–202.
[26] Y. Bai, H. Si, Experimental study on feeding characteristics of conical bottom pneumatic spout feeder for biomass pyrolysis, Chem. Eng. Process. Process Intensif. 166 (2021), 108490.
[27] B. Tan, Z. Huang, Z. Yin, X. Min, Y.G. Liu, X. Wu, M. Fang, Preparation and thermal properties of shape-stabilized composite phase change materials based on polyethylene glycol and porous carbon prepared from potato, RSC Adv. 6 (2016) 15821–15830.
[28] D. Carpenter, T. Westover, D. Howe, S. Deutch, A. Starace, R. Emerson, S. Hernandez, D. Santosa, C. Lukins, I. Kutnyakov, Catalytic hydroprocessing of fast pyrolysis oils: impact of biomass feedstock on process efficiency, Biomass Bioenergy 96 (2017) 142–151.
[29] J.A. Lacey, J.E. Aston, T.L. Westover, R.S. Cherry, D.N. Thompson, Removal of introduced inorganic content from chipped forest residues via air classification, Fuel 160 (2015) 265–273.
[30] M.B. Griffin, K. Iisa, H. Wang, A. Dutta, K.A. Orton, R.J. French, D.M. Santosa, N. Wilson, E. Christensen, C. Nash, Driving towards cost-competitive biofuels through catalytic fast pyrolysis by rethinking catalyst selection and reactor configuration, Energy Environ. Sci. 11 (2018) 2904–2918.
[31] D. Howe, T. Westover, D. Carpenter, D. Santosa, R. Emerson, S. Deutch, A. Starace, I. Kutnyakov, C. Lukins, Field-to-Fuel Performance Testing of Lignocellulosic Feedstocks: An Integrated Study of the Fast Pyrolysis–Hydrotreating Pathway, Energy Fuel 29 (2015) 3188–3197.
[32] R.J. Evans, T.A. Milne, Molecular characterization of the pyrolysis of biomass, Energy Fuel 1 (1987) 123–137.
[33] W. Jin, J.L. Klinger, T.L. Westover, H. Huang, A density dependent Drucker-Prager/Cap model for ring shear simulation of ground loblolly pine, Powder Technol. 368 (2020) 45–58.
[34] J. Klinger, N. Saha, T. Bhattacharjee, S. Carilli, W. Jin, Y. Xia, R. Daniel, C. Burns, O. Ajayi, Z. Cheng, Multiscale shear properties and flow performance of milled woody biomass, Front. Energy Res. 10 (2022).
[35] K. Lê Thành, J.-M. Commandré, J. Valette, G. Volle, M. Meyer, Detailed identification and quantification of the condensable species released during torrefaction of lignocellulosic biomasses, Fuel Process. Technol. 139 (2015) 226–235.

[36] G.S. Pullman, M. Buchanan, Identification and quantitative analysis of stage-specific organic acids in loblolly pine (*Pinus taeda* L.) zygotic embryo and female gametophyte, Plant Sci. 170 (2006) 634–647.
[37] J. Kesselmeier, K. Bode, U. Hofmann, H. Müller, L. Schäfer, A. Wolf, P. Ciccioli, E. Brancaleoni, A. Cecinato, M. Frattoni, P. Foster, C. Ferrari, V. Jacob, J.L. Fugit, L. Dutaur, V. Simon, L. Torres, Emission of short chained organic acids, aldehydes and monoterpenes from *Quercus ilex* L. and *Pinus pinea* L. in relation to physiological activities, carbon budget and emission algorithms, Atmos. Environ. 31 (1997) 119–133.
[38] A.E. Harman-Ware, M.F. Davis, G.F. Peter, Y. Wang, R.W. Sykes, Estimation of terpene content in loblolly pine biomass using a hybrid fast-GC and pyrolysis-molecular beam mass spectrometry method, J. Anal. Appl. Pyrolysis 124 (2017) 343–348.